International Journal of Thermal Sciences 49 (2010) 1183–1192

Contents lists available at ScienceDirect

International Journal of Thermal Sciences

journal homepage: www.elsevier.com/locate/ijts

Heat transfer, flow regime and instability of a nano- and micro-porous structure evaporator in a two-phase thermosyphon loop

Rahmatollah Khodabandeh*, Richard Furberg

Department of Applied Thermodynamics and Refrigeration, Institution of Energy Technology, School of Industrial Engineering and Management, Royal Institute of Technology (KTH), Stockholm, Sweden

ARTICLE INFO

Article history:
Received 15 July 2009
Received in revised form
13 January 2010
Accepted 14 January 2010
Available online 13 February 2010

Keywords:
Instability
Thermosyphon loop
Natural circulation
Heat transfer
Electronic cooling
Nano- and micro-porous structure surfaces

ABSTRACT

Two-phase flow instabilities which may occur at low and high heat loads were studied for a thermosyphon loop with R134a as refrigerant. The heat transfer surface of the evaporator was enhanced with a copper nano- and micro-porous structure. The heat transfer of the enhanced evaporator was compared to a smooth surface evaporator. Finally, the influence of the liquid level and the inside diameter of the riser on the instability of the system have been investigated.

It was found that the enhanced structure surface decreased the oscillations at the entire range of heat fluxes and enhanced the heat transfer coefficient. Three flow regimes were observed: Bubbly flow with nucleate boiling heat transfer mechanism, confined bubbly/churn flow with backflow and finally churn flow at high heat fluxes.

1. Introduction

In order to meet the growing cooling demand of electronic components, due to increasing heat fluxes and size constraints, different liquid cooling technologies have been proposed, such as heat pipe, thermosyphon, spray and jet impingement. Thermosyphon cooling as a passive system is able to dissipate high heat fluxes at relatively small temperature differences between the evaporator and condenser. As a heat removal system, a thermosyphon loop enhances passive safety by eliminating the need for a recirculation pump that is normally present in conventional cooling systems. The key parameters which influence the performance of the system, such as system pressure, pressure drop at different part of the thermosyphon, choice of working fluid and the various thermal resistances at different part of the system have been investigated by the author and co-authors [1–4].

Methods for producing efficient boiling surfaces have been investigated by using micro- and nano-structured surfaces. Formation of these structures may provide both surface enlargement and additional artificial nucleation sites which improve the heat transfer coefficient, and in many cases, improve the CHF. Enhanced surfaces such as herringbone, micro-fin and cross-grooved structures have been investigated by many researches and have been found to enhance the heat transfer. Bergles [5] has identified more than thirteen enhancement techniques which can be used for different applications. Honda et al. [6] presented the effects of micro-pin-fins and submicron-scale roughness on the boiling heat transfer using FC-72 as the working fluid and found that the micro-pin-fin chips enhanced heat transfer, boiling incipience and CHF and also the submicron-scale roughness improved the heat transfer for both plain and pin-fin chips. The advantage of cylindrical copper micro-structure surfaces in heat pipes was investigated by Akapiev et al. [7]. Ramaswamy et al. [8,9], Ghiu and Joshi [10,11] studied micro-channels with various channel widths, pitches, and heights. The new surfaces showed improvement of the heat transfer coefficient, incipience of the boiling point and CHF. Theofanous [12,13] studied the thermal patterns on nanoscopically smooth surfaces and found that nano-scale imperfections and defects present on the heater were sufficient to initiate the heterogeneous nucleation. Vemuri and Kim [14] investigated the advantages of nano-sized surface structure in pool boiling of working fluid FC-72, while Kang [15] studied effects of surface roughness on pool boiling heat transfer.

The thermal performance of a thermosyphon was improved with the use of fabricated surface structure in the evaporator, as shown by Khodabandeh and Palm [16] Nakayama et al. [17] and Ramaswamy et al. [18].

* Corresponding author. Tel.: +46 8 7907413.
E-mail address: rahmat@energy.kth.se (R. Khodabandeh).

1290-0729/$ – see front matter © 2010 Elsevier Masson SAS. All rights reserved.
doi:10.1016/j.ijthermalsci.2010.01.016

Nomenclature

A	heat transfer area
CHF	critical heat flux
D_h	hydraulic diameter
DC	Direct current
DR	Diameter riser
fps	Frame per second
H	channel height
h	heat transfer coefficient (W/cm^2 K)
L	channel length
LL	liquid level
Q	heat load (W)
q	heat flux (W/cm^2)
T	temperature (°C)
T_{evap_avg}	average evaporator surface temperature
T_{sat}	refrigerant saturation temperature
w	channel width
ΔT	Temperature difference between average evaporator temperature and the saturation temperature of test fluid

One of the main challenges with the use of thermosyphons for electronic cooling is to predict and control the oscillations during different heat loads. The aim of this study is to investigate the oscillating behavior during unstable operation of an experimental two-phase closed thermosyphon loop with an evaporator enhanced with a nano- and micro-porous surface structure.

Within reactor cooling technology several studies have been conducted to address two-phase flow stability for both low and high heat loads. Griffith [19], in the early 1960s, described the geysering. Aritomi et al. [20] and Chiang et al. [21] described three types of instabilities, geysering, natural circulation oscillations and density wave oscillations. Prasad et al. [22] classified the instabilities in two-phase flow with natural circulation as dynamic and static. Static instabilities referred to steady state characteristics of the system like boiling crises, flow pattern transition and excursion, whereas the dynamic stabilities were caused by feedback mechanisms such as density wave oscillations which were generated when the flow rate, vapor generation rate and pressure drop in boiling channel interact at a specific condition. Tadrist [23] classified the thermal oscillations, pressure drop oscillations and parallel channel instabilities as dynamic instabilities. Nayak et al. [24,25] investigated instabilities of an advanced heavy water reactor and found, among other, that type I instability occurs at channel exit quality less than 10% and as sub-cooling increases the instability also increases.

It has been shown by Furuya et al. [26,27] that flashing occurrence during boiling is of importance for type I instability.

Van der Hagen et al. [28] reported characteristics of type I and type II instabilities based on experimental results and simulation codes.

Kruijf et al. [29] found that the stability of the natural circulation improves as the heat power is increase for low sub-cooling values.

Jiang et al. [30] and Yang et al. [31] discussed flow excursion phenomenon and its mechanism in a wide range of sub-cooling at different flow modes for a natural circulation loop.

Yun et al. [32] used homogeneous model simulation to investigate the instability of a natural circulation loop and found an instability region at low pressure and quality.

Chang and Lahey [33] developed an analytical model for analysis of chaotic instabilities in boiling system.

Prasad et al. [22] developed a numerical model of boiling-water reactor for simulation of instabilities and found that increasing the mass flow rate or decreasing the power input does not necessarily stabilize the boiling at low Froud number.

Chiang et al. [34] investigated the transient behavior of natural circulation. They found that if the condensation rate was higher than the circulation rate then reversal flow and geysering were induced. By increasing the system pressure, geysering was suppressed and the region where the oscillation occurs became narrower.

2. Experimental setup

The thermosyphon loop consisted of an evaporator and a condenser connected by two tubes: a riser and a down-comer. Fig. 1 shows a schematic drawing of the thermosyphon and some of its important dimensions. The general layout of the evaporator can be found in Fig. 2. The evaporator was made of a small copper block in which a single rectangular channel was milled. In order to facilitate the visualization of flow regime in the evaporator channel a transparent polycarbonate window was attached to the evaporator. Two different evaporators channel were tested: one with a nano- and micro-porous structure (n-μ-p) and the other one with smooth surface. Channel dimensions of the tested evaporator, calculated hydraulic diameter, D_h, and the heat transfer surface area, A, can be find in Table 1. As it is shown in Fig. 2 the evaporator wall temperature was measured at three different locations. The thermocouples, with a diameter of 0.6 mm, were first coated with a high conductivity silver epoxy before being inserted in the 5 mm deep holes.

The average channel temperature was used for the analysis of the evaporator. The evaporator holder, which was made of steel, held the evaporator section by four screws and bolts. The evaporator was separated from the holder by two layers of rubber and a Teflon gasket to insulate the evaporator from the holder. The condenser was designed as a water cooled coaxial tube where, by adjusting the cooling water temperature and flow rate, the system pressure was controlled. The coaxial tube condenser was 1 m long with a 16 mm diameter water tube and 9.5 mm refrigerant tube. The cooling water was supplied by an adjustable cooling machine with a DC pump to control the flow rate of the water and to achieve desirable water temperature. In order to investigate the influence of

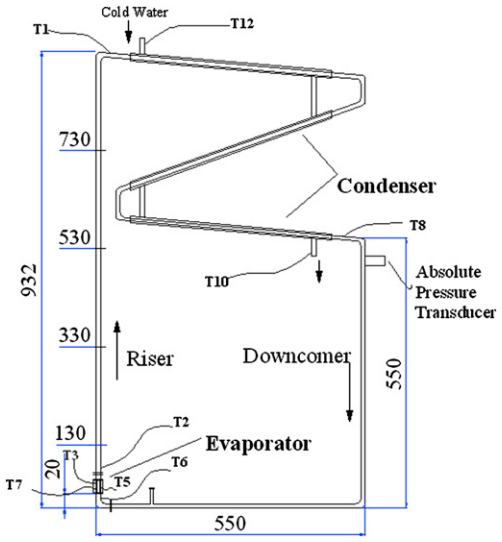

Fig. 1. A schematic drawing of experimental setup. All distances are in mm.

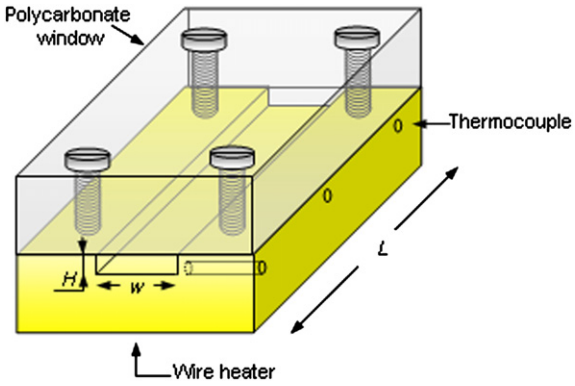

Fig. 2. A general layout of evaporator with polycarbonate window.

liquid level on the performance and instability of the thermosyphon system, the liquid level of 330, 530 and 730 mm were used. To further understand the instability, the tests were run with three different glass tube risers of 10, 7.7 and 4 mm. The heater was constructed from a coiled Ni–Chrome wire, which was attached at the backside of the evaporator by using a thin layer of high resistant cement to insulate the wire from the copper evaporator. Moreover to decrease the loss of heat from wire to the outside, the heater and the evaporator backside were heavily insulated. The heat load was obtained from the electric current and voltage as measured by the power supplier (TTi, EX752M MULTI-MODE PSU). Type T thermocouples were used for the temperature measurements.

As it is shown in Fig. 1, temperatures were measured at the inlet and the outlet of condenser and evaporator, along the channel as well as the inlet and outlet water. Tests were conducted with R134a as the working fluid at reduced pressure of 0.16, corresponding to 6.5 bar, and a saturation temperature of approximately 24.2 °C. The system pressure inside the thermosyphon was measured at the outlet of the condenser by an electronic pressure transducer (Druck PDCR 960, 10 bar). The evaporator channel was filmed with a high speed video camera (Redlake, MotionXtra, HG-LE) with a Navitar 12× macro zoom lens. Two 250 W tungsten lamps (Dedocool dedolight) were used as light sources. Most films were taken with a frame rate of 1000–2000 fps and with a length of about 0.5–1 s.

3. Data acquisition

A data logger was used to record the temperature and pressure measurements. For each heat load, the thermosyphon was allowed to run until all measurements were stable, where in the case of instabilities, with a certain periodic fluctuations. When steady state was reached, the temperatures and pressure were recorded each second until 40 separate measurements had been taken. The averages of these values were used to calculate the heat transfer coefficient. The evaporator wall temperatures were measured at three different locations and an average of these values was used as the temperature of the evaporator. Degree of fluctuation (Figs. 7, 12 and 14, 16) was calculated as maximum deviation (±) between the average of 40 values and the local one. The heat transfer coefficient was calculated according to equation (1).

Table 1
Channel dimensions of the tested evaporators.

Evaporator	L (mm)	H (mm)	W (mm)	D_h (mm)	A (cm^2)
H-1.6	30.0	1.6	5.1	2.4	2.49
n-*μ*-*p*-H-1.7	30.0	1.7	5.1	2.5	2.50

$$h = \frac{Q}{A \cdot \Delta T} \tag{1}$$

where Q is the heat load measured from voltage and current from the power supplier unit, A is the apparent heat transfer channel area, which was calculated according to equation (2).

$$A = (2H + w) \bullet L \tag{2}$$

The dimensions of the channel were measured with computer imaging software, by analyzing close-up pictures of the channel with a micrometer reference in the picture. The temperature difference, ΔT, was defined as the difference between the average evaporator temperature, T_{evap_avg}, and the saturation temperature from the measured saturation pressure, calculated by the software EES (Engineering Equation Solver). Degree of sub-cooling at the inlet of the evaporator was presented in Table 2. In order to ensure quality of the measured values, the estimated uncertainty and the expected uncertainty and the overall uncertainty were calculated. The uncertainty of the heat transfer coefficient was affected by errors in the measurement and fluctuation of the wall temperature, the liquid bulk temperature, the heated surface area and the heat dissipation. Estimated uncertainties are characterized by the concept of standard deviation. The expected uncertainty for the temperature difference was considered as 0.1 °C. Table 3 presented the uncertainty of each variable and also the heat transfer coefficient as combined uncertainty. The value for the temperature difference was based on estimated and expected uncertainties.

The uncertainty of the temperature difference and the surface area contributed mostly to the overall uncertainty of the heat transfer coefficient. It should be noted that, for the most heat fluxes the uncertainty of the temperature difference was much lower which result in lower overall uncertainty than the maximum value presented in the table.

4. Nano- and micro-porous structure surface

The nano- and micro-porous structure was manufactured on the entire surface of the evaporator channel. The manufacturing technique was shown by Furberg [35], where electrodeposition was used to build up these novel three-dimensional structures. As it is shown in Fig. 3 the channel evaporator was used as the cathode and a copper plate was used as the anode. The two electrode surfaces were fixed in the electrolyte and supplied by a constant DC current. During the deposition dendritic copper structure grows shown by

Table 2
Degree of sub-cooling ($\Delta t = T_s - T_f$).

q (W/cm^2)	Smooth	Nano	LL-33; DR-10	LL-53; DR-10	LL-73; DR-10	LL-33; DR-4	LL-53; DR-4
2	−0.3	−0.2	0.9	−0.4	1.7	0.0	−0.4
5	0.1	−0.1	0.8	2.0	1.8	−0.4	2.0
10	0.0	0.0	0.7	3.1	2.2	0.0	3.1
15	0.2	0.1	0.7	3.5	1.7	1.6	3.5
16						2.8	
17			0.5				
18						3.4	
20	0.3	0.1		3.7	1.6	3.5	3.7
22						4.1	
25	0.3	0.0		3.8	1.8		3.8
30	0.3	0.1		4.0	2.0		4.0
35	0.3	0.1		4.0	1.9		4.0
40	0.4	0.2					
45	0.2	0.3					
46	0.4						
48	0.2						
50		0.3					

Table 3
Uncertainty of heat transfer coefficient, h, based on different variables.

	Smooth	Nano	LL-33; DR-10	LL-53; DR-10	LL-73; DR-10	LL-33; DR-4	LL-53; DR-4
U	0.30%	0.30%	0.30%	0.30%	0.30%	0.30%	0.30%
I	0.60%	0.60%	0.60%	0.60%	0.60%	0.60%	0.60%
$(DT)_{max}$	5.90%	3.50%	3.40%	3.30%	3.3%	4.2%	3.5%
L	0.30%	0.30%	0.30%	0.30%	0.30%	0.30%	0.30%
H	2.90%	2.90%	2.90%	2.90%	2.90%	2.90%	2.90%
w	1.50%	1.50%	1.50%	1.50%	1.50%	1.50%	1.50%
Combined uncertainty%	6.8	4.8	4.8	4.7	4.7	5.4	4.8

Fig. 5 as hydrogen bubbles interact on the copper particles. The 'pores' size of the deposited copper structure increases when the hydrogen bubbles depart from the copper surface and merge into bigger bubbles. In order to produce the desired structure, the main parameters, current density, time, temperature, and pressure were controlled during the deposition process. SEM (scanning electron microscope) pictures of the tested surface are shown in Figs. 4 and 5.

As seen in Fig. 4, the micro-sized pores had an average top layer pore diameter of about 110 μm with an approximate pore density of 30 pores/mm^2. The thickness of the surface layer measured about 250 μm. The dendritic wall structure featured numerous small cavities in the size of only a few hundred nanometers. In this study, the submicron particles were grown and stabilized to about 2 μm (Fig. 5), to ensure good thermal conductivity through the structure and robust mechanical stability.

5. Experimental results and discussion

5.1. Instability

According to Niro and Beretta [36], fully developed boiling occurs when waiting time for bubble is much shorter than the growth time. With intermittent boiling the waiting time for new bubbles is much longer than the growth time. With long waiting time for bubbles the liquid superheats and cause sudden explosive nucleation and formation of large bubbles. Bubbles collapse as sub-cooled liquid flows into the inlet of evaporator or in the unheated riser. The temperature of the evaporator wall gradually increases during waiting time and decreases during growth time of the bubbles. During the waiting time for new bubbles, sub-cooled liquid flows back into the evaporator which decreases the evaporator wall temperature and pressure. Instead of continuous boiling, boiling occurs in a certain period (intermittent boiling) with a pulsation character.

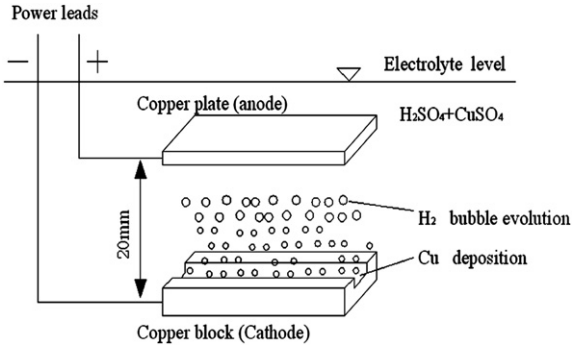

Fig. 3. Fabrication of the nano- and micro-porous structure by deposition process.

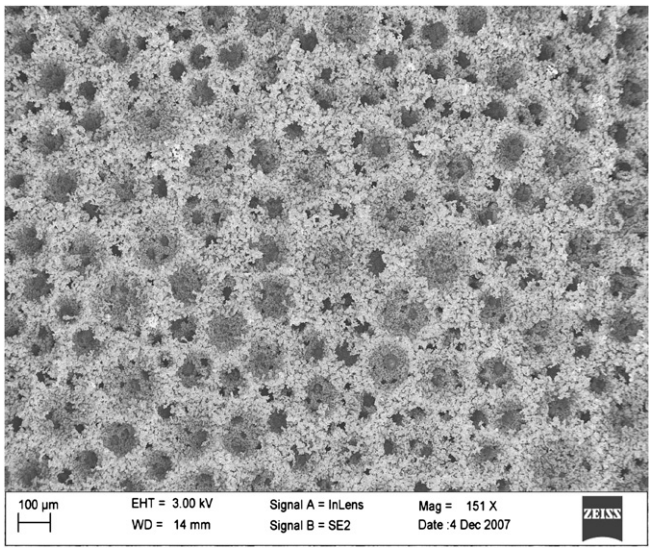

Fig. 4. SEM picture of nano- and micro-porous structure surface.

As Vijayan and Nayak [37] discussed instabilities in the literature are presented in different ways, i.e. based on analysis method where the instability threshold can be predicted by using governing equations, propagation method, nature of oscillations, geometry and so on. Instabilities classified according to propagation method are restricted to dynamic instabilities where the mechanism associates with the propagation or transport of disturbances in the system. In a two-phase thermosyphon loop the disturbances can be transported by density (or void) waves. With a given geometry, increase of a heat flux causes higher void fraction which leads to increasing driving force and flow rate. The enlarged flow rate reduces the exit enthalpy and the void fraction which gives higher density of the mixture at the outlet of the evaporator. This increase and decrease of mixture density in the loop with an appropriate time delay and magnitude is described as density wave oscillation which may occurs in both low (type I) and high (type II) heat fluxes. Additional description of the instability is associated with boiling inception at low heat flux where the boiling inception causes disturbance that can bring changes in the density and the driving force in a natural circulation loop. Flashing instability and geysering

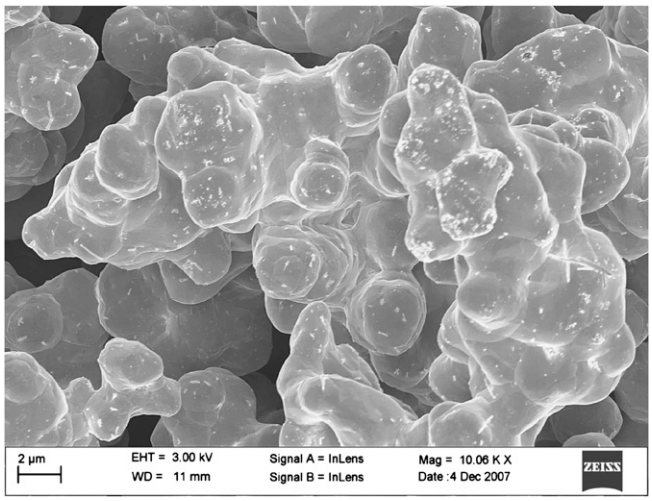

Fig. 5. SEM picture of nano-porous structure contrast with lengths of 2 μm.

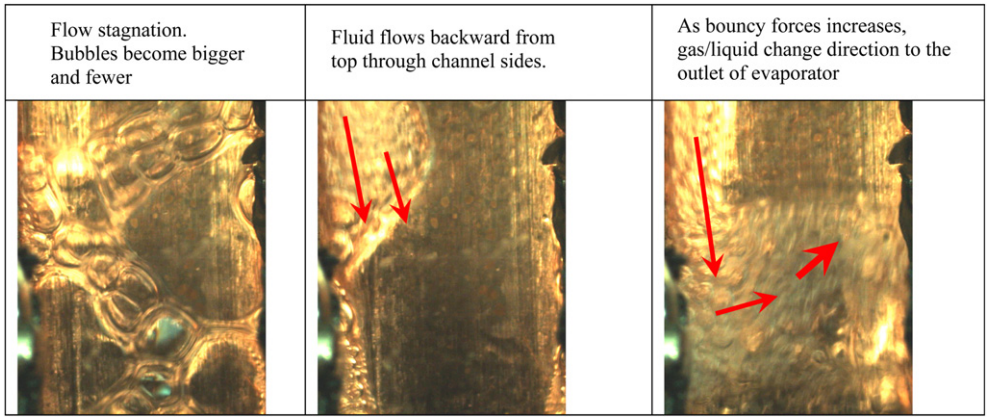

Fig. 6. Flow stagnation, backflow and upward flow.

is described in this category. Flow excursion (static instability) is known as Ledinegg instability which a sudden decrease in flow rate induces the occurrence of CHF. Distinctive feature of this instability is the occurrence of multiple steady state solutions. In transition boiling regime the wetting and drying of the heating surface gives oscillation of surface temperature which is known as boiling crisis instability. Flow pattern transition instability refers to differences in pressure drop in different flow regime. In slug flow which has higher pressure drop than annular flow, with increased heat flux the vapor fraction increases and the flow regime is shifted to annular flow. Due to the lower pressure drop in the annular flow the flow rate increases resulting in lower exit enthalpy and decreasing of the vapor fraction and the change of flow pattern to slug flow.

As discussed above various bases are used for classification of the instabilities. The same instability can be explained with different classification. In this study propagation method based on density wave oscillation was used to describe the instabilities in the thermosyphon system. Two types of instabilities, type I and type II instability, were observed from the video recordings and the temperature measurements. Both instabilities occurred due to an inefficient heat transfer, but for different reasons. Type I occurred at start up, as expected at relatively low heat fluxes. This was caused mainly by backflow of liquid from riser and also condensed vapor in the evaporator with flow stagnation in evaporator in the first step and totally collapse of vapor in the second step which gave single phase flow in evaporator with much lower heat transfer. In the third step, the bubbles initiated, grew and departed from the surface and thereby cooled down the evaporator wall (Fig. 6). Periodic fluctuations of the wall temperature due to the flow instability, referred to type I where the system was not in steady state with periodic changing of increasing and decreasing of the wall temperature at a certain frequency. Fig. 6 shows typical behavior of backflow, flow stagnation and upward flow which cause type I instability. Type II instability occurred at high heat fluxes at relatively high friction two-phase flow pressure drop at slug/churn flow regime with convective heat transfer mechanism. This instability with high heat fluxes was related to disturbed nucleate boiling and occurrence of hot dry spots and also convective mechanism of the heat transfer. As the vapor quality increased and the boiling suppressed, dry patches form locally and the wall temperature increased. Temperature measurements in three different locations in the evaporator channel showed that the heat transfer at the inlet was more efficient with lower wall temperature as compared to the middle and outlet of the evaporator where the occurrence of dried hot spot were less feasible.

Furberg et al. [38] showed that the novel nano- and micro-porous surfaces enhanced pool boiling heat transfer with over 10 times compared to a plain copper surface. Visualization with the aid of the high speed camera showed that the number and the frequency of the produced bubbles were apparently higher for the novel nano- and micro-porous surfaces compared to the smooth surface.

For the enhanced surfaces due to enhanced turbulence and continuous boiling with high frequency generated enough bubbles to cause sufficient density difference between riser and downcomer to ensure the required mass flow for the smooth running of the thermosyphon system. On the other hand it was suggested that low nucleation frequencies bring intermittent boiling regime which was the main reason for thermal instability. Intermittent boiling was caused by backflow and backflow appeared due to condensation or collapse of bubbles.

Observations from this study, in terms of boiling delay and instability was in accordance with results presented by Niro and Beretta [36] for smooth surface channel.

As it presented in Table 1, the channel dimensions of the smooth and nano- and micro-porous surfaces were essentially the same. The fluctuations presented in Fig. 7 were maximum deviation from average measured temperatures in the wall channel of the evaporator. As seen in Fig. 7, the enhancement structure surface decreased the oscillations at around 10 and 45 W/cm^2. Up to

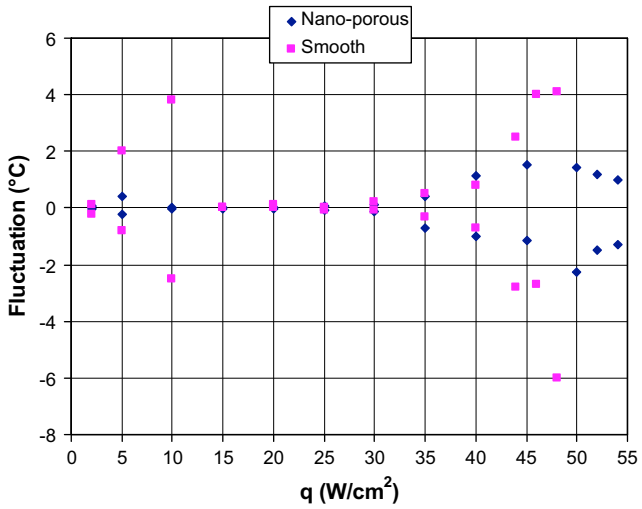

Fig. 7. Fluctuation of evaporator wall temperature based on maximum deviation from the average at different heat fluxes with 7.7 mm diameter riser for nano–micro-porous and smooth surfaces.

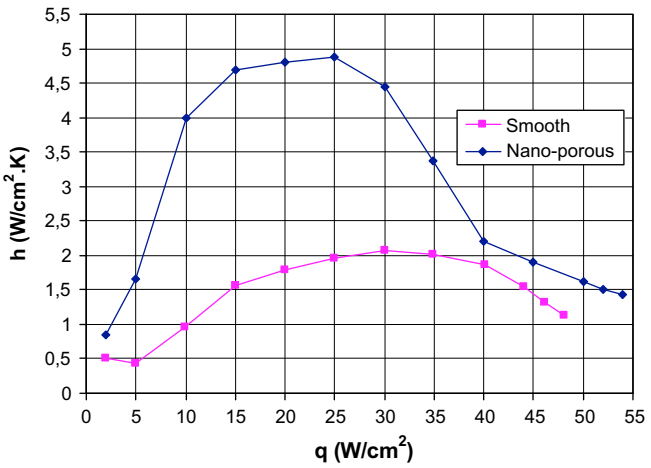

Fig. 8. Heat transfer coefficient versus heat flux for the smooth and nano- and micro-porous evaporator with diameter riser of 7.7 mm.

35 W/cm^2 the maximum deviations from the average value was less than 1 °C, while at higher heat fluxes it was increased gradually.

Oscillations at low and high heat fluxes occurred with the smooth surface. Low heat flux, the smooth surface produced low vapor fraction which, in combination with intermittent boiling in the evaporator, and backflow caused oscillations. Fig. 7 shows thermal instability for the smooth surface which appeared in the range of 5–10 W/cm^2 and also with heat fluxes above 35 W/cm^2. Type I instability was characteristic of low heat fluxes, while at higher heat fluxes than 35 W/cm^2 type II instability was dominant, due to the transition into convective heat transfer mechanism and occurrence of dried hot spot.

At moderate heat fluxes (15–35 W/cm^2), nucleation frequency and vapor fraction increased and the buoyancy forces of the vapor slugs suppressed the backflow and lifted the refrigerant into the condenser. At higher heat fluxes than 35 W/cm^2, the video analysis did not show the backflow, but unsteady behavior was observed for both smooth and nano- and micro-porous structure surfaces as seen in Fig. 7. More nucleation sites with the high porosity for the nano- and micro-structure surface wall gave less oscillation compared to the smooth wall surface.

5.2. Heat transfer

The heat transfer coefficient results from smooth and nano- and micro-porous structure surface were presented in Fig. 8. In accordance with previous experiments, presented by Furberg et al. [39] the heat transfer coefficient was significantly enhanced, up to 4 times by using nano- and micro-porous structure compared to the smooth surface at a heat flux of 10 W/cm^2. The maximum heat transfer coefficient of about 4.8 (W/cm^2 K) for the nano- and micro-porous surface was recorded at 25 W/cm^2.

Three main characteristics of the structure of the enhanced surfaces were discussed by Furberg et al. [38]. Firstly, due the high density and shape of the channel the produced vapor during evaporation inside the structure could be released with low resistance from the dendritic structure. Secondly, the high porosity of the structure trapped vapor and assisted the progress of liquid transport and also promoted the communication between active nucleation sites. Thirdly, the dendritically shaped, with its large surface area, probably assisted the formation of thin liquid films which promoted the evaporation rate and heat transfer coefficient.

Decreasing the heat transfer coefficient and increasing the thermal instability in higher heat fluxes than 30 W/cm^2 for nano- and micro-porous structure (Figs. 7 and 8) can be explained either by high liquid velocity which disturb and suppress the nucleation sites or simply vapor patches trapped in the structure. At higher heat fluxes, form a churn like flow with much lower heat transfer coefficient expressed convective evaporation where alternate dry patches and rewetting of the evaporator channel caused oscillation of the temperature.

As seen in Fig. 8 the heat transfer coefficient increased with increasing the heat flux up to 25–30 W/cm^2 (in the region of bubbly flow regime) for nano- and micro-porous respectively smooth surfaces which indicated nucleate boiling heat transfer mechanism. The bubbly flow regime was dominated by nucleate boiling whereas the slug/churn flow was controlled by convective evaporation which was independent on the heat flux. In the range of low heat flux oscillations for both surfaces the bubbly flow was disturbed by backflow which lead to intermittent boiling with confined bubbly- and slug flow with formation of the large bubble which filled the channel and decreased the circulation rate as it discussed earlier.

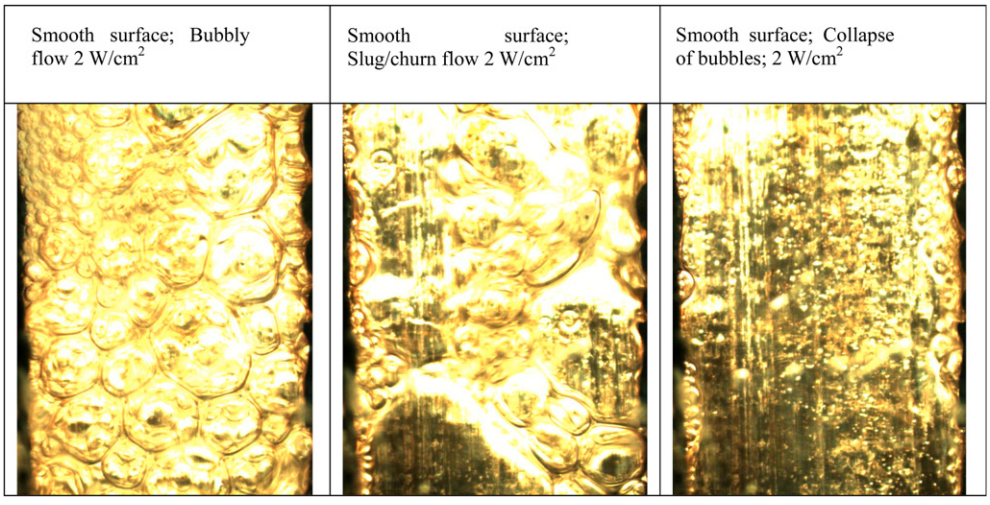

Fig. 9. Images of flow regimes for a typical complete cycle for 2 W/cm^2 for smooth surface.

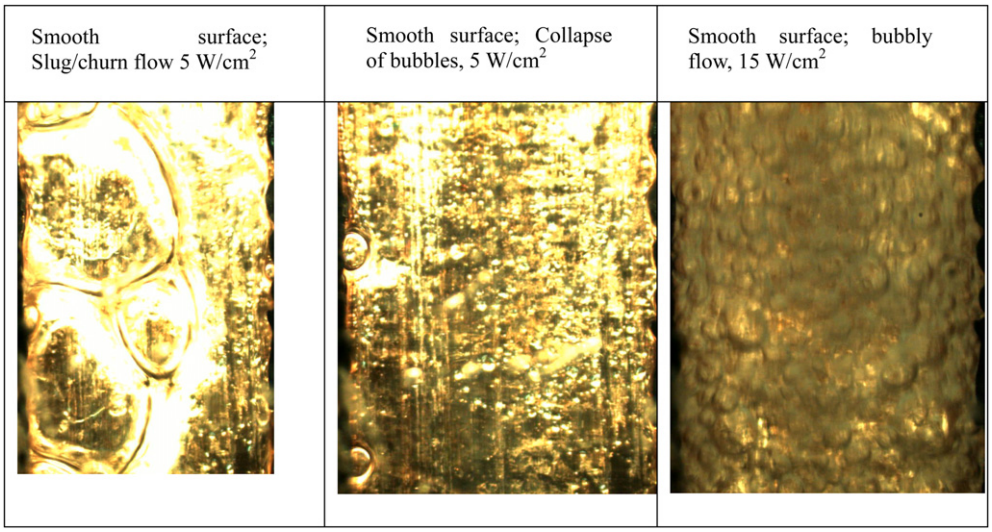

Fig. 10. Video images of flow regimes for smooth surface at 5 W/cm^2 and 15 W/cm^2.

5.3. Flow regime

A complete cycle for 2 W/cm^2 may be divided into four steps (Fig. 9). In the first step the bubbles were produced and during production of bubbles the flow regime was bubbly flow (Fig. 9, video image in the left). In second step the produced bubbles became larger and coalescenced with other bubbles forming a large bubble where the flow regime seemed to be slug flow (Fig. 9, video image in the middle). In the third step large bubbles collapsed due to liquid backflow into the evaporator and formed a thin liquid film (Fig. 9, image in right). In the last step, the thin liquid film evaporated and the channel was partly dried. During this step with increasing the wall temperature, the superheated liquid which flowed from the bottom of the evaporator, evaporated rapidly and cooled down the evaporator channel and the cycle was completed. Despite the transition of flow regime during a complete cycle the dominant flow regime could be considered as bubbly flow. At 5 W/cm^2 the bubbles grew, merged and collapsed at higher rate and the dominant flow regime could be considered as confined bubbly/slug flow which was shown in Fig. 10 (figures in the left and middle). The right video image in Fig. 10 was displayed a typical flow regime (bubbly flow) in the range of 15–35 W/cm^2. The left image in Fig. 11 showed churn/annular flow at heat flux ranges larger than 35 W/cm^2. For the nano- and micro-porous structure surface bubbly flow up to 35 W/cm^2 (right image in Fig. 11) observed with the exception of 5 W/cm^2 (middle video image at Fig. 11) where tendency to confined bubbly/slug flow was displayed.

5.4. Influence of liquid level on the performance of the thermosyphon system with nano-porous structure surface

As can be seen in Fig. 12 the oscillations at low heat fluxes (2–5 W/cm^2) for all three liquid levels were very low but increased at 10–17 W/cm^2 for liquid level of 33 cm. Observations from high speed video camera for this liquid level showed bubbly flow, coalescence of bubble, building of slug and finally collapse of bubbles and slugs at the top of liquid head which did not reach the inlet of the condenser. Intermittent boiling by periodically flowing of vapor/liquid and liquid to the outlet of the evaporator resulted in

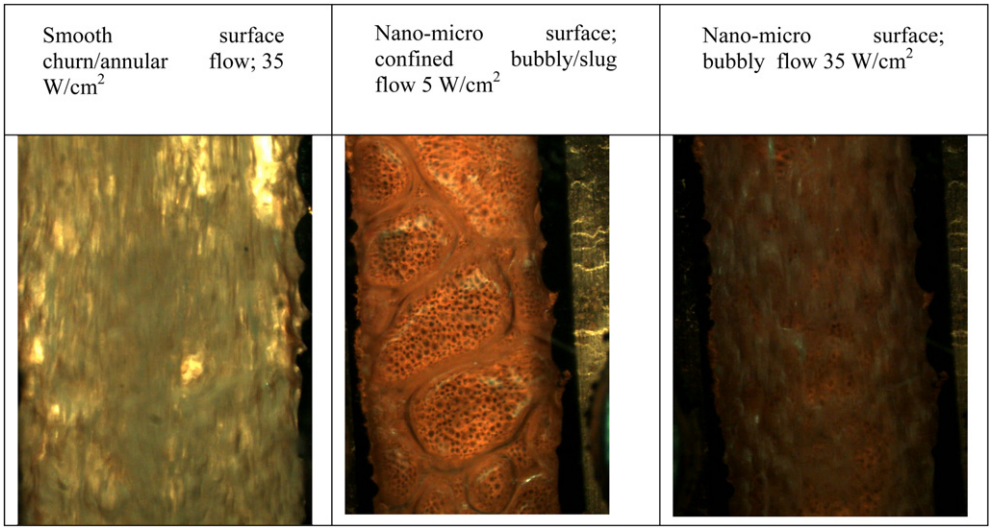

Fig. 11. Video images of flow regimes for smooth and nano–micro-surfaces at different heat fluxes.

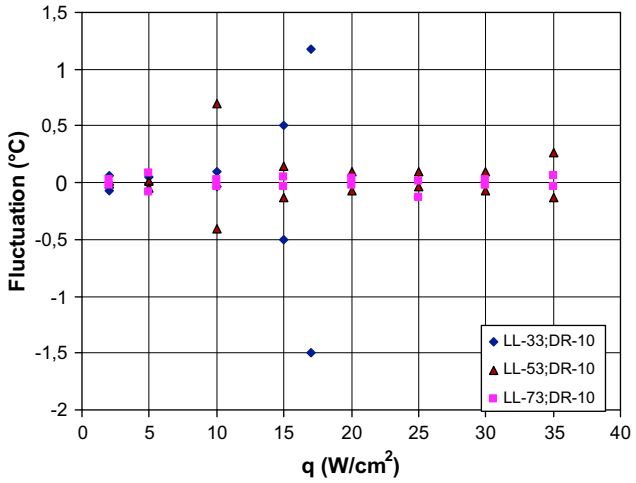

Fig. 12. Fluctuation of evaporator wall temperature based on maximum deviation from the average at different heat fluxes for nano- and micro-porous surface at different liquid level (LL) with a diameter riser (DR) of 10 mm.

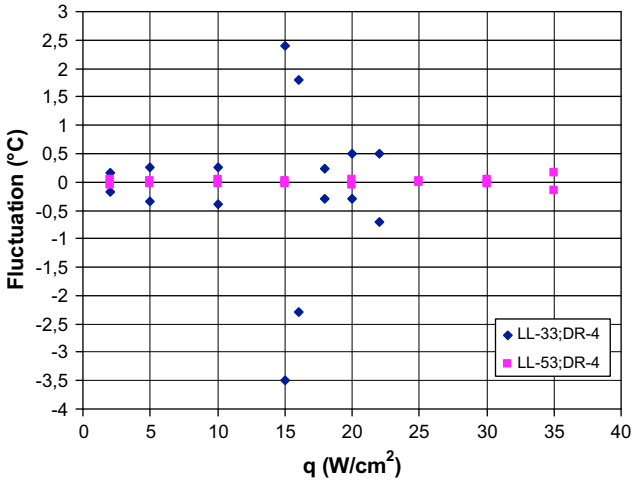

Fig. 14. Fluctuation of evaporator wall temperature based on maximum deviation from the average at different heat fluxes for nano–micro-porous surface at two different liquid levels (LL) with a diameter riser (DR) of 4 mm.

thermal instability and instable heat transfer. Here the liquid head was not enough to lift the gas/liquid to the condenser.

It should be noted that due to the high fluctuations and increased wall temperature the tests for liquid level of 33 cm were stopped at 17 W/cm^2. Same figure showed higher fluctuations for liquid levels of 53 cm than 73 cm. The higher liquid level delivered higher mass flow rate and flowing force (mass flow multiplied by gas/liquid velocity in the riser) which easier lifted up the liquid/gas column from the riser to the condenser with lower backflow. Due to the larger flowing force and undisturbed nucleation in the evaporator the heat transfer coefficient was increased (Fig. 13) and the fluctuations were suppressed. At the smallest liquid level (33 cm) for low heat fluxes (2–10 W/cm^2) the fluctuations were rather low. Tests were interrupted at higher heat fluxes due to early occurrence of type II instability with churn flow with rapidly decreased heat transfer coefficient. It should be pointed out that the 17 W/cm^2 should not be considered as the CHF for this liquid level. In another study with smooth surface it was found similar behavior in the heat transfer and instability at same heat fluxes. With increased heat fluxes the instabilities decreased and the heat transfer coefficient increased, but at much lower degree than the liquid levels of 53 and 73 cm.

5.5. Influence of liquid level and diameter of riser on oscillations and heat transfer

As the liquid level was reduced to 33 cm with riser diameter of 4 mm the fluctuation was increased as seen in Fig. 14. Temperature measurements demonstrated the dominant of the type I instability at 15 W/cm^2 while at 16 W/cm^2 the magnitude of both types were almost the same. With higher heat fluxes than 16 W/cm^2 type I instability suppressed while the type II remained constant.

A comparison of Fig. 12 (DR = 10 mm) and 14 (DR = 4 mm) showed a reduction of oscillation by introducing smaller diameter of riser channel for liquid level of 53 cm, while the behavior of the 33 cm liquid level with few measured available data seemed to be rather the opposite.

A comparison of Fig. 13 (DR = 10 mm) and Fig. 15 (DR = 4 mm) for liquid level of 33 cm showed decreased heat transfer at higher heat fluxes than 10 W/cm^2. At higher heat fluxes than 20 W/cm^2 the

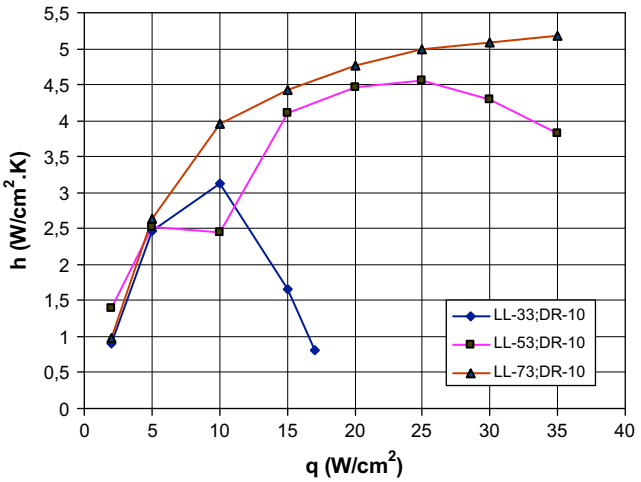

Fig. 13. Heat transfer coefficient at different heat fluxes for nano–micro-porous surface at different liquid level (LL) with a diameter riser (DR) of 10 mm.

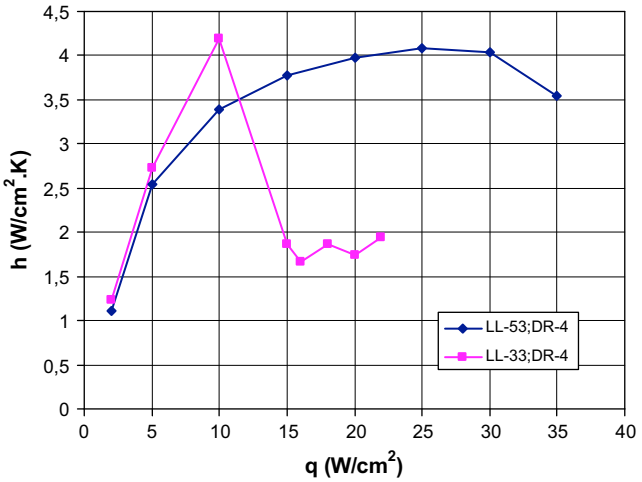

Fig. 15. Heat transfer coefficient at different heat fluxes for nano–micro-porous surface at two different liquid levels (LL) with a diameter riser (DR) of 4 mm.

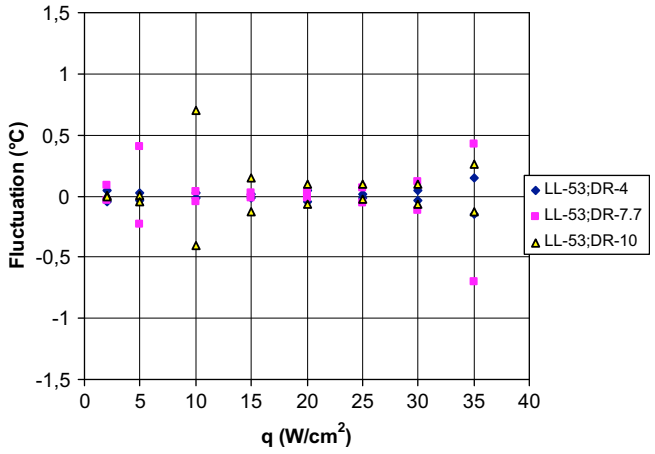

Fig. 16. Fluctuation of evaporator wall temperature based on maximum deviation from the average at different heat fluxes for nano–micro-porous surface at same liquid level (LL) and different diameter of the riser (DR).

behavior of the system was rather unclear due to interruption of the experiment.

The larger the diameter of riser the more oscillation occurred in the evaporator as can be seen in Fig. 16. Previously reported mass flow simulation [2] of the thermosyphon system showed almost constant mass flow at same liquid level. The reduction of cross-section of the riser provided higher gas/liquid flow in the riser which facilitated the lift of two-phase flow into condenser, preventing backflow. From observing the two-phase flow mixture in the riser, it was clear that the flowing force was too small to push all liquid to the condenser at heat fluxes where large fluctuations occurred. As a result, the fluctuations decreased with a reduction of the cross-section of the riser and the oscillations were more pronounced at 10 and 7.7 mm diameter of the riser.

Fig. 17 showed that the 7.7 mm diameter riser gave the highest heat transfer performance at 10–30 W/cm^2. However the heat transfer for 10 mm was better than 4 mm in the range of 15–35 W/cm^2. Visualization from high speed video camera confirmed the more occurrence of backflow which caused oscillations and lower heat transfer with 10 mm riser compared to 7.7 mm diameter of the riser. At the range of 10–30 W/cm^2 bubbly flow, with negligible fluctuations, gave high heat transfer for 7.7 mm.

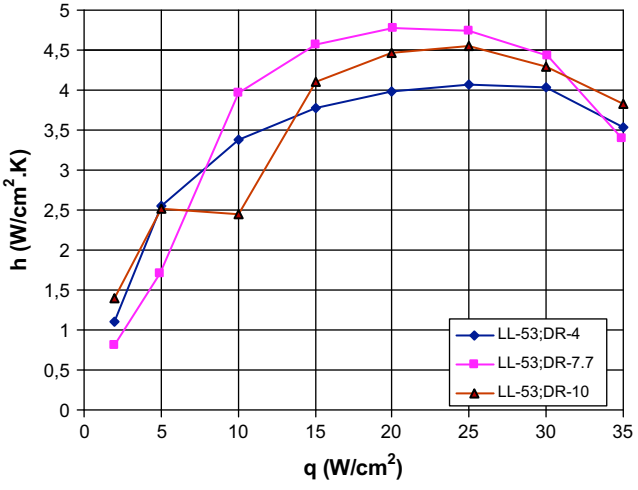

Fig. 17. Heat transfer coefficient at different heat fluxes for nano–micro-porous surface at same liquid level (LL) and different diameter of the riser (DR).

In spite of lowest oscillations for 4 mm diameter riser the heat transfer was lower in the range of 15–30 W/cm^2 than two other dimensions. The lower heat transfer was probably attributed to two main reasons. Firstly, 4 mm diameter riser caused considerably higher friction pressure drop than two other tested dimensions which reduced the mass flux through the thermosyphon. Hence, dryout occurred early in the evaporator. Secondly, the slope of increasing heat transfer coefficient with increasing heat flux was lower which indicated more convective evaporation than two other cases with a lower heat transfer as the result. Probably an optimum of the diameter riser gives best performance where the high pressure drop should be avoided, and on the other hand the flowing force should be enough large to lift up the liquid in the riser into the condenser without bubble collapses and backflow.

6. Conclusion

It was found that the enhanced structure surface decreased the oscillations at the entire range of heat fluxes and enhanced the heat transfer coefficient due to higher nucleation density and bubble frequency. Two different instabilities were observed. Both occurred due to an inefficient heat transfer in boiling and evaporation but for different reasons. Type I instability occurred at low heat fluxes where the backflow was presented. Type II instability was showed at high heat fluxes where the nucleate boiling mechanism was suppressed, dry patches formed and the temperature of the evaporator fluctuated due to rewetting and dryout of evaporator wall temperature.

Generally three flow regimes were observed: Bubbly flow with nucleate boiling heat transfer mechanism whereas heat transfer increased with increasing heat flux, confined bubbly/churn flow with backflow and low heat transfer coefficient and finally churn flow at high heat fluxes with convective evaporation.

Higher liquid level in the riser improved the performance of the thermosyphone and suppressed fluctuations. It was found that, the larger the cross-section of the riser the more oscillation occurred in the evaporator which was due to lower flowing force to lift up the liquid in the riser to the condenser. Generally at lower liquid level and larger diameter of the riser at low heat fluxes, vapor/liquid in the riser was not able to reach the condenser inlet, rather the bubbles and slugs collapsed in the riser and build up a fluctuating liquid column in the riser.

Acknowledgments

The authors would like to thank Yongtian Xu for his contribution in the measurements and also express our gratitude to Prof. Mamoun Muhammed, Dr Muhammet Toprak and Dr Shanghua Li for helping to make the nano- and micro-porous structured surface at the division of Functional Material Technology at Royal Institute of the Technology (KTH).

References

[1] R. Khodabandeh, B. Palm, Influence of system pressure on the boiling heat transfer coefficient in a closed two-phase thermosyphon loop. International Journal of Thermal Sciences 41 (2002) 619–624 Elsevier.
[2] R. Khodabandeh, Pressure drop in riser and evaporator in an advanced two-phase thermosyphon loop. International Journal of Refrigeration 28 (2005) 725–734.
[3] B. Palm, R. Khodabandeh, Choosing working fluid for two phase thermosyphon systems for cooling of electronics. Transactions of the ASME, Journal of Electronic Packaging (June 2003) 276–281.
[4] R. Khodabandeh, Thermal performance of a closed advanced two-phase thermosyphon loop for cooling of Radio Base Stations at different operating conditions. Journal of Applied Thermal Engineering 24 (2004) 2643–2655.

[5] A.E. Bergles, V. Nirmalan, G.H. Junkhan, R.L. Webb, Bibliography on Augmentation of Convective Heat and Mass Transfer II Heat Transfer Laboratory Report HTL-31, ISU-ERI-Ames-84221. Iowa State University, December 1983.
[6] H. Honda, H. Takamatsu, J.J. Wei, Enhanced boiling of FC-72 on silicon chips with micro-pin-fins and submicron-scale roughness. Journal of Heat Transfer 124 (2002) 383–390.
[7] G.N. Akapiev, S.N. Dmitriev, B. Erler, V.V. Shirkova, A. Achultz, H. Pietsch, Ion track membranes providing heat pipe surfaces with capillary structures. Nuclear Instruments and Methods in Physics Research Section B: Beam Interactions with Materials and Atoms 208 (2003) 133–136.
[8] C. Ramaswamy, Y. Joshi, W. Nakayama, W.B. Johnson, High speed visualization of boiling from an enhanced structure. International Journal of Heat and Mass Transfer 45 (2002) 4761–4771.
[9] C. Ramaswamy, Y. Joshi, W. Nakayama, W.B. Johnson, Semi-analytical model for boiling from enhanced structures. International Journal of Heat and Mass Transfer 46 (2003) 4257–4269.
[10] C.D. Ghiu, Y. Joshi, Visualization study of pool boiling from thin confined enhanced structures. International Journal of Heat and Mass Transfer 78 (2005) 4287–4299.
[11] C.D. Ghiu, Y. Joshi, Boiling performance of single-layered enhanced structures. Journal of Heat Transfer 127 (2005) 675–683.
[12] T.G. Theofanous, J.P. Tu, A.T. Dinh, T.N. Dinh, The boiling crisis phenomenon: part 1: nucleation and nucleate boiling heat transfer. Experimental Thermal and Fluid Science 26 (2002) 775–792.
[13] T.G. Theofanous, J.P. Tu, A.T. Dinh, T.N. Dinh, The boiling crisis phenomenon: part II: dryout dynamics and Burnout. Experimental Thermal and Fluid Science 26 (2002) 793–810.
[14] S. Vemuri, K.J. Kim, Pool boiling of saturated FC-72 on nano-porous surface. International Communications in Heat and Mass Transfer 32 (2005) 27–31.
[15] M. Kang, Effect of surface roughness on pool boiling heat transfer. International Journal of Heat and Mass Transfer 43 (2000) 4073–4085.
[16] R. Khodabandeh, B. Palm, An experimental investigation of the influence of threaded surface on the boiling heat transfer coefficients in vertical narrow channels. Microscale Thermophysical Engineering 6 (2) (April 01, 2002) 131–139.
[17] W. Nakayama, T. Nakajima,S. Hirasawa, Heat Sink Studs Having Enhanced Boiling Surfaces for Cooling of Microelectronic Component, ASME Paper No. 84-WA/HT-89, 1984.
[18] C. Ramaswamy, Y. Joshi, W. Nakayama, W.B. Johnson, Compact thermosyphons employing microfabricated component. Microscale Thermophysical Engineering 3 (1999) 273–282.
[19] P. Griffith, Geysering in Liquid-filled Lines, ASME, Paper 62-HT-39, 1962.
[20] M. Aritomi, J.H. Chiang, M. Mori, Geysering in parallel boiling channels. Nuclear Engineering and Design 141 (1993) 111–121.
[21] J.H. Chiang, M. Aritomi, M. Mori, Fundamental study on thermo-hydraulics during start-up in natural circulation induced by hydrostatic head fluctuation. Journal of Nuclear Science and Technology 30 (3) (1993) 203–211.
[22] R.O.S. Prasad, J.B. Doshi, Kannan Iyer, A numerical investigation of nuclear coupled density wave oscillations. Nuclear Engineering and Design 154 (1995) 381–396.
[23] L. Tadrist, Review on two-phase flow instabilities in narrow spaces. International Journal of Heat and Fluid Flow 28 (2007) 54–62.
[24] A.K. Nayak, P.K. Vijayan, D. Saha, V. Venkat Raj, Masanori Aritomi, Analytical study of nuclear-coupled density-wave instability in a natural circulation pressure tube type boiling water reactor. Nuclear Engineering Design 195 (2000) 27–44.
[25] A.K. Nayak, P.K. Vijayan, D. Saha, V. Venkat Raj, Masanori Aritomi, Study on the stability behaviour of a natural circulation pressure tube type boiling water reactor. Nuclear Engineering Design 215 (2002) 127–137.
[26] M. Furuya, F. Inada, A. Yasuo, Density wave oscillations of a boiling natural circulation loop induced by flashing, in: Proc. NURETH-7 (International Meeting on Nuclear Reactor Thermal–Hydrualics), 1995, pp. 923–932.
[27] M. Furuya, F. Inada, T.H.J.J. Van der Hagen, Flushing-induced density wave oscillations in a natural circulation BWR-mechanism of instability and stability map. Nuclear Engineering and Design 235 (2005) 1557–1569.
[28] T.H.J.J. Van der Hagen, A.J.C. Stekelenburg, D.D.B. Van Bragt, Reactor experiments on type 1 and type 2 BWR stability. Nuclear Engineering and Design 200 (2000) 177–185.
[29] W.J.M. de Kruijf, T. Sengstag, D.W. de Haas, T.H.J.J. van der Hagen, Experimental thermohydraulic stability map of a Freon-12 boiling water reactor facility with high exit friction. Nuclear Engineering and Design 229 (2004) 75–80.
[30] S.Y. Jiang, Y.J. Zhang, X.X. Wu, J.H. Bo, H.J. Jia, Flow excursion phenomenon and its mechanism in natural circulation. Nuclear Engineering and Design 202 (2000) 17–26.
[31] X.T. Yang, S.Y. Jiang, Y.J. Zhang, Mechanism analysis on flow excursion of a natural circulation with low steam quality. Nuclear Engineering and Design 235 (2005) 2391–2406.
[32] G. Yun, G.H. Su, J.Q. Wang, W.X. Tian, S.Z. Qiu, D.N. Jia, J.W. Zhang, Two-phase instability analysis in natural circulation loops of China advanced research reactor. Annals of Nuclear Energy 32 (2005) 379–397.
[33] C.J. Chang, R.T. Lahey Jr., Analysis of chaotic instabilities in boiling system. Nuclear Engineering and Design 167 (1997) 307–334.
[34] J.H. Chiang, M. Aritomi, R. Inoue, M. Mori, Thermo-hydraulics during start-up in natural circulation boiling water reactors. Nuclear Engineering and Design 146 (1994) 241–252.
[35] R. Furberg, Enhanced boiling heat transfer from a novel nanodendritic microporous copper structure, ISSN: 1102-0245, Licentiate Thesis at Royal Institute of Technology, Stockholm, Sweden.
[36] A. Niro, G.P. Beretta, Boiling regimes in a closed two-phase thermosyphon. International Journal of Heat and Mass Transfer 33 (10) (1990) 2099–2111.
[37] R.K. Vijayan, A.K. Nayak, Introduction to instabilities in natural circulation systems, Annex7, Reactor Engineering Division, Bhabha Atomic Research Centre, India.
[38] R. Furberg, S. Li, B. Palm, M. Toprak, M. Muhammed, Dendritically ordered nano-particles in a micro-porous structure for enhanced boiling, in: Proceedings IHTC-13 Conference, Sydney, Australia, August 2006, pp. 13–18.
[39] R. Furberg, R. Khodabandeh, B. Palm, S. Li, M. Toprak, M. Muhammed, Experimental investigation of an evaporator enhanced with micro-porous structure in a two-phase thermosyphon loop, in: Proceedings of 2008 ASME Summer Heat Transfer Conference HT2008, August 10–14, 2008, Jacksonville, Florida, USA.